

Two-gap superconductivity in $\text{Mo}_8\text{Ga}_{41}$ and its evolution upon the V substitution

V.Yu. Verchenko,^{1,2} R. Khasanov,³ Z. Guguchia,³ A.A. Tsirlin,⁴ and A.V. Shevelkov¹

¹*Department of Chemistry, Lomonosov Moscow State University, 119991 Moscow, Russia**

²*National Institute of Chemical Physics and Biophysics, 12618 Tallinn, Estonia*

³*Laboratory for Muon Spin Spectroscopy, Paul Scherrer Institute, CH-5232 Villigen PSI, Switzerland†*

⁴*Experimental Physics VI, Center for Electronic Correlations and Magnetism, Institute of Physics, University of Augsburg, 86135 Augsburg, Germany*

Zero-field and transverse-field muon spin rotation/relaxation (μSR) experiments were undertaken in order to elucidate microscopic properties of a strongly-coupled superconductor $\text{Mo}_8\text{Ga}_{41}$ with $T_c = 9.8\text{ K}$. The upper critical field extracted from the transverse-field μSR data exhibits significant reduction with respect to the data from thermodynamic measurements indicating the coexistence of two independent length scales in the superconducting state. Accordingly, the temperature-dependent magnetic penetration depth of $\text{Mo}_8\text{Ga}_{41}$ is described using the model, in which two s -wave superconducting gaps are assumed. The V for Mo substitution in the parent compound leads to the complete suppression of one superconducting gap, and $\text{Mo}_7\text{VGa}_{41}$ is well described within the single s -wave gap scenario. The reduction in the superfluid density and the evolution of the low-temperature resistivity upon the V substitution indicate the emergence of a competing state in $\text{Mo}_7\text{VGa}_{41}$ that may be responsible for the closure of one of the superconducting gaps.

PACS numbers: 74.25.Bt, 74.70.Ad, 76.75.+i

I. INTRODUCTION

Design of new superconducting materials following empirical rules based on chemical and structural considerations or rigorous analysis of the electronic structure is a challenging task. Recently, systematic work was performed on superconducting intermetallics with endohedral gallium clusters TGa_n (T is a transition metal)¹. In this context, $\text{Mo}_8\text{Ga}_{41}$ ² (the superconducting transition temperature $T_c \simeq 9.7\text{ K}$), $\text{Mo}_6\text{Ga}_{31}$ ³ ($T_c \simeq 8\text{ K}$), ReGa_5 ¹ ($T_c \simeq 2.3\text{ K}$), Rh_2Ga_9 ⁴ ($T_c \simeq 1.9\text{ K}$) and Ir_2Ga_9 ⁴ ($T_c \simeq 2.2\text{ K}$) superconductors as well as non-superconducting V_8Ga_{41} ⁵ and PdGa_5 ⁶ are considered. By analyzing their electronic structures, Xie *et al.*¹ established the interrelations between the critical temperature T_c and valence electron count, thus placing these structurally different intermetallic compounds into an individual class of superconductors.

$\text{Mo}_8\text{Ga}_{41}$ was firstly synthesized by Yvon *et al.*⁷ during their systematic investigation of Ga-rich intermetallic compounds with unusual crystal structures. View of the $\text{Mo}_8\text{Ga}_{41}$ crystal structure is shown in Fig. 1. The crystal structure is built by MoGa_{10} polyhedra, which are condensed on the triangular faces of GaGa_{12} cuboctahedron. A detailed description of the crystal structure can be found elsewhere⁸. From the first sight, $\text{Mo}_8\text{Ga}_{41}$ follows all of the Matthias' empirical rules for superconductors: it contains a $4d$ transition metal (Mo), the compound may possess high density of electronic states, and its complex crystal structure is closely related to the cubic symmetry. Despite the fact that nowadays these rules seem to be obsolete, Yvon and co-authors² found that $\text{Mo}_8\text{Ga}_{41}$ superconducts below $T_c = 9.7\text{ K}$ with the upper critical field of $\mu_0 H_{c2} = 8.6\text{ T}$. Results obtained by Yvon *et al.* were further pointed out on the unusual behavior of $\text{Mo}_8\text{Ga}_{41}$ in its superconducting state. Indeed, val-

ues of T_c and dH_{c2}/dT lead to the Werthamer-Helfand-Honenberg (WHH) prediction of the upper critical field $\mu_0 H_{c2} \simeq 6.7\text{ T}$, which is significantly smaller than the experimental value². Together with a relatively high critical temperature, this may indicate strong electron-phonon coupling in the superconducting regime.

In our recent study⁸, we carried out comprehensive investigation of thermodynamic and transport properties of $\text{Mo}_8\text{Ga}_{41}$ in both, the normal and superconducting, states. Magnetization, heat capacity, and resistivity measurements confirmed bulk superconductivity at $T_c = 9.8\text{ K}$ in zero magnetic field. The superconducting transition was found to be characterized by a large value of the normalized specific heat jump $\Delta c_p / \gamma_N T_c = 2.84$, which is twice as high as the weak-coupling BCS prediction. At the same time, the electronic contribution to the specific heat below T_c obeyed a power-law rather than exponential decay behavior as is expected within the framework of BCS theory. Such disagreements have motivated us for further investigation of microscopic properties of $\text{Mo}_8\text{Ga}_{41}$.

Here, we present the results of muon spin rotation/relaxation (μSR) experiments on bulk $\text{Mo}_8\text{Ga}_{41}$ and its V-substituted derivative, $\text{Mo}_7\text{VGa}_{41}$. Transverse-field μSR (TF- μSR) experiments were undertaken in order to elucidate superconducting-state properties of both materials. The temperature-dependent magnetic penetration depth λ and the upper critical field $\mu_0 H_{c2}$ were extracted from the TF- μSR data and were used to investigate the order parameter in $\text{Mo}_8\text{Ga}_{41}$ and its evolution upon the V for Mo substitution.

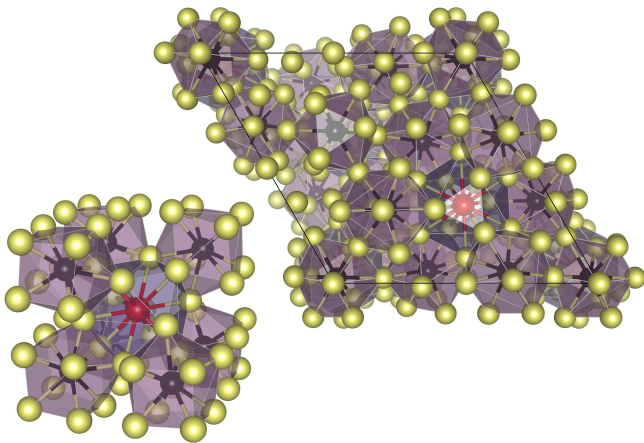


FIG. 1. View of the $\text{Mo}_8\text{Ga}_{41}$ crystal structure: (left) eight MoGa_{10} polyhedra surrounding the GaGa_{12} cuboctahedron (one polyhedron is not shown for clarity); (right) polyhedral representation of the unit cell. Mo atoms are shown in black color, Ga atoms in yellow color, and the unique Ga atom in the center of cuboctahedron – in red color.

II. EXPERIMENTAL DETAILS

$\text{Mo}_8\text{Ga}_{41}$ and $\text{Mo}_7\text{VGa}_{41}$ specimens were synthesized as described earlier⁸ in the form of small submillimeter-size crystals. Elemental composition of the obtained crystals was investigated using a JSM JEOL 6490-LV scanning electron microscope operated at 30 kV and equipped with an energy-dispersive x-ray detection system INCA x-Sight. For quantitative analysis, molybdenum and vanadium elements, and gallium phosphide provided by MAC Analytical Standards were used as external standards. According to the EDX spectroscopy results, crystals of $\text{Mo}_8\text{Ga}_{41}$ and $\text{Mo}_7\text{VGa}_{41}$ contain 16.3(5) at. % Mo, 83.7(8) at. % Ga, and 14.4(5) at. % Mo, 2.0(2) at. % V, and 83.6(9) at. % Ga, respectively, leading to the $\text{Mo}_{8.0(2)}\text{Ga}_{41.0(4)}$ and $\text{Mo}_{7.1(2)}\text{V}_{1.0(1)}\text{Ga}_{41.0(4)}$ formula units. In the case of $\text{Mo}_7\text{VGa}_{41}$ ⁹, elemental mapping was used to check the distribution of Mo and V species across the surface, which was found to be uniform confirming local homogeneity of crystals. For measurements of thermodynamic properties, several crystals of $\text{Mo}_7\text{VGa}_{41}$ were glued together and measured as a polycrystalline sample. Magnetization curves were registered in magnetic fields between 0 T and 14 T at temperatures between 1.8 K and 10 K using the VSM setup of a Physical Property Measurement System (PPMS, Quantum Design). Heat capacity was measured in magnetic fields up to 12 T by the relaxation method using the Heat Capacity option of PPMS. Further, crystals of $\text{Mo}_8\text{Ga}_{41}$ and $\text{Mo}_7\text{VGa}_{41}$ were crushed by grinding in an agate mortar and analyzed by powder x-ray diffraction technique. The experiments were performed on a Huber Guinier Camera G670 [Image plate detector, Cu x-ray source, Ge (111) monochromator, $\lambda = 1.540598 \text{ \AA}$]. PXRD patterns of $\text{Mo}_8\text{Ga}_{41}$ and $\text{Mo}_7\text{VGa}_{41}$ agree with the V_8Ga_{41}

structure type and show no impurity phases in the specimens. Finally, the obtained powders of $\text{Mo}_8\text{Ga}_{41}$ and $\text{Mo}_7\text{VGa}_{41}$ were pressed into cylindrical pellets with the diameter of 6 mm and the height of 1 mm at room temperature at the external pressure of 100 bar. These pellets were used for the μSR experiments.

μSR measurements were performed at the Paul Scherrer Institute (PSI), Villigen, Switzerland. Zero-field (ZF) and transverse-field (TF) μSR experiments were carried out on the GPS and DOLLY spectrometers located at the πM3 and πE1 beamlines, respectively. Experiments were performed in the temperature range from 1.6 to 15 K in GPS and from 0.29 to 15 K in DOLLY instruments. ZF- μSR experiments were performed in zero applied field. In TF- μSR experiments the sample was field-cooled from above T_c in series of fields ranging from 30 mT to 0.59 T.

III. RESULTS AND DISCUSSION

A. $\text{Mo}_8\text{Ga}_{41}$

1. Zero-field μSR experiments

Figure 2 shows ZF- μSR time-spectra of $\text{Mo}_8\text{Ga}_{41}$ measured at $T = 0.29 \text{ K}$ and 12.5 K . The obtained spectra below and above T_c reveal no significant difference indicating the absence of internal coherent magnetic fields in $\text{Mo}_8\text{Ga}_{41}$ that may appear, for instance, as a result of long-range magnetic ordering. On the contrary, our ZF- μSR data show that the only nuclear component is present, which can be analyzed by using the static Kubo-Toyabe depolarization function¹⁰:

$$A(t) = A_s(0) \left[\frac{1}{3} + \frac{2}{3} (1 - \sigma_{\text{KT}}^2 t^2) \exp\left(-\frac{\sigma_{\text{KT}}^2 t^2}{2}\right) \right] + A_{\text{bgd}}, \quad (1)$$

where $A_s(0)$ is the initial asymmetry for muons stopped in the sample, σ_{KT} is the muon depolarization rate, and A_{bgd} is the background contribution from muons that missed the sample. The muon depolarization rate σ_{KT} does not change with temperature within its standard deviation (see the inset in Fig. 2). This clearly indicates the absence of any spontaneous coherent magnetic fields in the superconducting state of $\text{Mo}_8\text{Ga}_{41}$.

2. Transverse-field μSR experiments

In order to elucidate microscopic properties of the superconducting state in $\text{Mo}_8\text{Ga}_{41}$, including the structure of superconducting gap, transverse-field μSR experiments were carried out in magnetic fields of 30, 70, 200, and 490 mT. Figure 3 shows TF- μSR time-spectra of $\text{Mo}_8\text{Ga}_{41}$ measured at $T = 0.29 \text{ K}$ and 10 K in $\mu_0 H = 30 \text{ mT}$. The spectrum below T_c clearly exhibits faster relaxation with respect to the spectrum at 10 K due to the

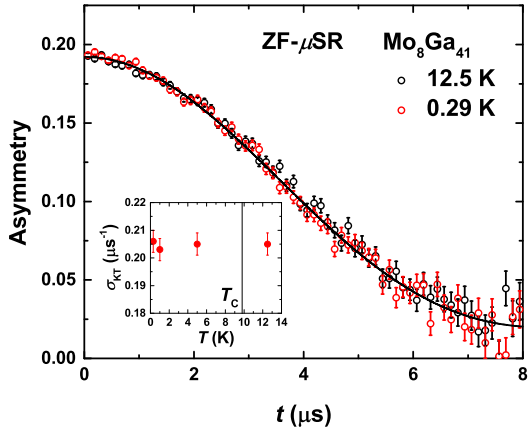


FIG. 2. ZF- μ SR time-spectra of $\text{Mo}_8\text{Ga}_{41}$ measured at $T = 0.29$ K and 12.5 K. Solid line is a fit of the $T = 12.5$ K data according to the Kubo-Toyabe relation (see in the text). The inset shows zero-field muon depolarization rate σ_{KT} as a function of temperature.

formation of the flux line lattice in the superconducting state. The following oscillatory decaying Gaussian function was used to fit the experimental data (the fitting results are shown as solid lines in Fig. 3):

$$A^{\text{TF}}(t) = A_s^{\text{TF}}(0) \times \exp\left(-\frac{\sigma^2 t^2}{2}\right) \times \cos(\gamma_\mu \mu_0 H_{\text{int}} t + \phi) + A_{\text{bgd}}^{\text{TF}}(0) \times \cos(\gamma_\mu \mu_0 H_{\text{bgd}} t + \phi). \quad (2)$$

Here, $A_s^{\text{TF}}(0)$ and $A_{\text{bgd}}^{\text{TF}}(0)$ are initial asymmetries belonging to the sample and the background contributions, respectively. $\gamma_\mu/2\pi = 135.5$ MHz/T is the muon gyromagnetic ratio, $\mu_0 H_{\text{int}}$ and $\mu_0 H_{\text{bgd}}$ are the internal and background magnetic fields, respectively, ϕ is the initial phase, and σ is the Gaussian muon spin relaxation rate. Above T_c , the muon spin relaxation rate is referred to the temperature independent nuclear magnetic dipolar contribution σ_{nm} , while below T_c , the total relaxation rate consists of the nuclear and superconducting contributions, $\sigma = \sqrt{\sigma_{\text{sc}}^2 + \sigma_{\text{nm}}^2}$. By fitting the data at $T = 10$ K, we obtained $\sigma_{\text{nm}} = 0.16 \mu\text{s}^{-1}$. This value was further used to extract $\sigma_{\text{sc}}(T)$ and $\mu_0 H_{\text{int}}(T)$ at temperatures below T_c according to Eq. 2. In the superconducting state, Fourier transforms of the asymmetry spectra are well described by the simple Gaussian approximation what is normally the case for powder samples of anisotropic superconductors. Fourier analysis of the asymmetry spectra shows no indications of disorder of the vortex lattice.

From the data taken at each temperature below the transition temperature T_c , we reconstructed σ_{sc} as a function of transverse field for $\mu_0 H = 30, 70, 200$ and 490 mT. The resulting $\sigma_{\text{sc}}(T)$ dependencies for various transverse fields are shown in Fig. 4. The temperature-dependent variation of σ_{sc} exhibits a clear enhancement below T_c .

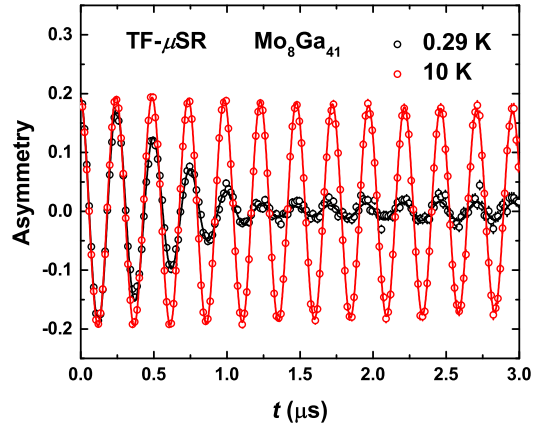


FIG. 3. TF- μ SR time-spectra of $\text{Mo}_8\text{Ga}_{41}$ measured in $\mu_0 H = 30$ mT at temperatures below (black dots) and above (red dots) the superconducting transition temperature. Solid lines are least-squares fits according to Eq. (2).

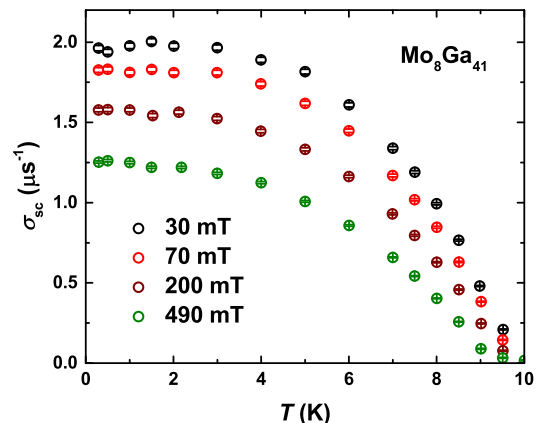


FIG. 4. Superconducting contribution σ_{sc} to the muon spin relaxation rate of $\text{Mo}_8\text{Ga}_{41}$.

Figure 4 also implies that σ_{sc} measured at similar temperatures decreases with increasing measuring field [see Fig. 5(a) where $\sigma_{\text{sc}}(\mu_0 H)$ at $T = 3$ K is depicted]. The more precise scan performed at $T = 1.7$ K shows that before coming down, σ_{sc} first increases by going through a maximum at around 20 mT [Fig. 5(b)]. Note that this is the typical behavior observed in various type-II superconductors experimentally¹¹ and as well as predicted theoretically¹².

In terms of Ginzburg-Landau treatment of the vortex state, Brandt¹² has shown that σ_{sc} can be calculated as a function of the reduced field b and the Ginzburg-Landau coefficient κ for the case of single-gap s -wave superconductivity:

$$\sigma_{sc} \approx 0.172 \frac{1-b}{\kappa^2} \left[1 + 1.21(1-\sqrt{b})^3 \right], \quad (3)$$

where $b = \frac{\mu_0 H}{\mu_0 H_{c2}}$, $\mu_0 H_{c2}$ is the upper critical field, $\kappa = \lambda/\xi$, λ is the magnetic penetration depth, and ξ is the Ginsburg-Landau coherence length. Eq. (3) is valid for b exceeding $0.25/\kappa^{1.3}$ (where the maximum of σ_{sc} occurs) and $\kappa \gtrsim 5$. For $\text{Mo}_8\text{Ga}_{41}$, the value of $\xi = 15.8$ nm was estimated from the upper critical field at zero temperature⁸, thus, Eq. (3) can be used for $\lambda > 79$ nm.

The $\sigma_{sc}(\mu_0 H)$ data obtained from T -scans [Fig. 5(a)] as well as from the $\mu_0 H$ -scan [Fig. 5(b)] were fitted using Eq. (3). Firstly, the fitting with $\mu_0 H_{c2}$ and λ treated as variable parameters (solid red lines in Fig. 5) was employed yielding the values of upper critical field $\mu_0 H_{c2}$ that are significantly smaller than that obtained from thermodynamic measurements previously⁸. Indeed, as shown in Fig. 5(a), by fitting the $\sigma_{sc}(\mu_0 H)$ data we obtained $\mu_0 H_{c2} = 3.77(4)$ T and $\lambda = 216.1(2)$ nm at $T = 3$ K, compared to 6.7 T from magnetization and heat-capacity measurements⁸. On the other hand, if such a high value of $\mu_0 H_{c2}$ is adopted, σ_{sc} has to be significantly enhanced, in poor agreement with the μ SR data. The same situation is observed in the case of $\mu_0 H$ -scan [Fig. 5(b)], where the values of $\mu_0 H_{c2} = 4.9(3)$ T and $\lambda = 215(1)$ nm were obtained at $T = 1.7$ K.

Values of the upper critical field of $\text{Mo}_8\text{Ga}_{41}$ are summarized in Fig. 6. Obviously, the entire plot of $\mu_0 H_{c2}(T)$ calculated from the TF- μ SR data exhibits large reduction in the upper critical field compared to thermodynamic measurements. This situation is a characteristic feature of multigap superconductivity that leads to two or more distinct length scales in the superconducting state¹³. Therefore, we further studied magnetic penetration depth in order to clarify this multigap behavior.

3. Magnetic penetration depth

The temperature-dependent inverse squared magnetic penetration depth λ^{-2} of $\text{Mo}_8\text{Ga}_{41}$ obtained from the TF- μ SR data using Eq. (3) is shown in Fig. 7. Upon increasing temperature, λ increases monotonically and tends to infinity at $T = T_c$. Concurrently, λ^{-2} decreases with increasing temperature and vanishes at the transition temperature. The temperature dependence of λ^{-2} is indicative of the order parameter, i.e., absolute value of the gap energy, as well as symmetry of the superconducting gap. Assuming weak-coupling BCS-type s -wave superconductivity with a single gap Δ reveals¹⁴

$$\frac{\lambda^{-2}(T)}{\lambda^{-2}(0)} = \frac{\Delta(T)}{\Delta(0)} \tanh \left[\frac{\Delta(T)}{2k_B T} \right], \quad (4)$$

in the dirty limit. At non-zero temperatures, the gap $\Delta(T)$ is assumed to follow the function $\Delta(T) =$

$\Delta(0) \tanh[1.82(1.018(T_c/T - 1))^{0.51}]$. This function has been found to well represent the temperature dependence at any coupling strength¹⁵.

The fit using Eq. (4) is shown in Fig. 7 as a dashed line. The single-gap BCS-type model satisfactorily describes the experimental data with $\Delta(0) = 1.80(7)$ meV, $\Delta(0)/k_B T_c = 2.1$, and $\lambda(0) = 192(2)$ nm. The reduced value of $\chi^2 = 0.66$ has been obtained with $n = 13$ degrees of freedom. The results of fitting, from the first sight, hint at the single-gap BCS-type superconductivity in $\text{Mo}_8\text{Ga}_{41}$. However, previously we established two non-BCS-type features⁸: (i) the superconducting state is characterized by the strong electron-phonon coupling with $\lambda_{ep} = 0.9$, (ii) the normalized specific heat jump $\Delta c_p/\gamma_N T_c = 2.84$ is much larger than in the weak-coupling BCS limit. Also, in the current study we found that (iii) the upper critical field from the TF- μ SR data shows the significant reduction with respect to the thermodynamic data. These features suggest that the single-gap BCS-type model should be avoided, and the multigap model should be used instead.

The two-gap model can be introduced using the linear combination of two s -wave superconducting gaps:

$$\frac{\lambda^{-2}(T)}{\lambda^{-2}(0)} = \omega \frac{\Delta_{s1}(T)}{\Delta_{s1}(0)} \tanh \left[\frac{\Delta_{s1}(T)}{2k_B T} \right] + (1-\omega) \frac{\Delta_{s2}(T)}{\Delta_{s2}(0)} \tanh \left[\frac{\Delta_{s2}(T)}{2k_B T} \right], \quad (5)$$

where ω is the linear combination coefficient describing the contribution of each gap, and $\Delta_{si}(T) = \Delta_{si}(0) \tanh[1.82(1.018(T_c/T - 1))^{0.51}]$ is the temperature dependence of each gap. Fit of the $\lambda^{-2}(T)$ data using Eq. 5 is shown as a solid red line in Fig. 7 yielding $\Delta_{s1}(0) = 4.3(6)$ meV, $\Delta_{s2}(0) = 1.76(6)$ meV, and $\lambda(0) = 216.2(4)$ nm. This fitting is characterized by the reduced value of $\chi^2 = 0.50$ with $n = 12$ degrees of freedom for $\omega = 0.7$. The value of ω was found during the least-squares fit and then was fixed in order to reduce possible correlations between parameters. The use of the two-gap model in comparison to the single-gap model slightly reduces the value of χ^2 with almost the same number of degrees of freedom. In the case of $\text{Mo}_8\text{Ga}_{41}$, the two-gap model implies the existence of two s -wave superconducting gaps with similar energies and almost equal contributions ($\omega = 0.7$). Certainly, this model replicates the single-gap BCS-type model when describing the $\lambda^{-2}(T)$ data, and the fitting results are very similar (compare the solid and dashed lines in Fig. 7). However, keeping in mind the non-BCS-type features listed above, we exclude the single-gap scenario from the consideration. At the same time, the $\lambda^{-2}(T)$ data corroborate the multigap behavior of $\text{Mo}_8\text{Ga}_{41}$ and reveal that the introduction of two superconducting gaps is sufficient to explain superconducting behavior of this compound. Note that similar behavior was reported for SrPt_3P , which was suggested to be a two-band superconductor with equal gaps¹⁶. Future studies that will help

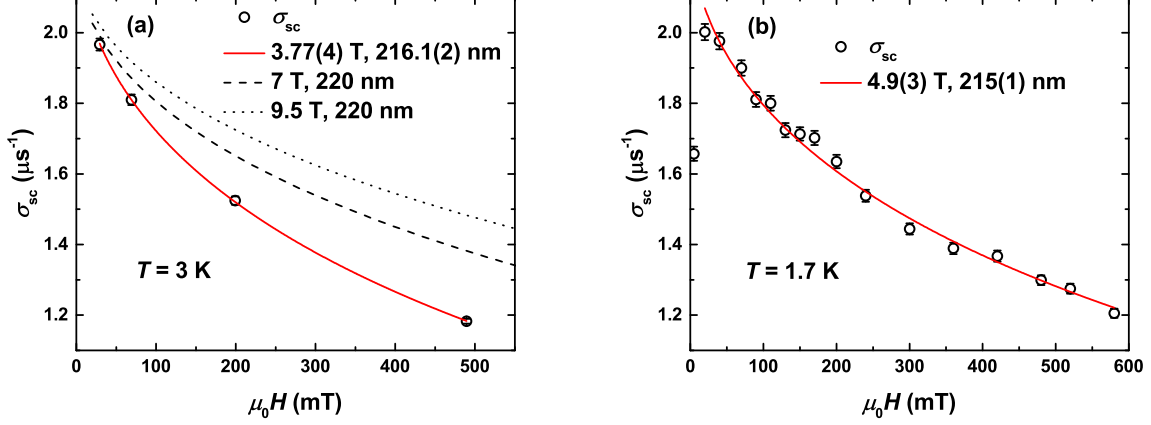


FIG. 5. (a) Field-dependent superconducting contribution σ_{sc} to the total muon spin relaxation rate of $\text{Mo}_8\text{Ga}_{41}$ taken from the TF- μSR T -scans at $T = 3$ K. Solid red line is a fit of the data according to Eq. (3) with $\mu_0 H_{c2}$ and λ treated as variable parameters, dashed and dotted lines are the results for $\mu_0 H_{c2} = 7$ T and $\mu_0 H_{c2} = 9.5$ T, respectively, and $\lambda = 220$ nm. (b) σ_{sc} obtained from the TF- μSR $\mu_0 H$ -scan at $T = 1.7$ K. The solid red line is a fit of the data according to Eq. (3).

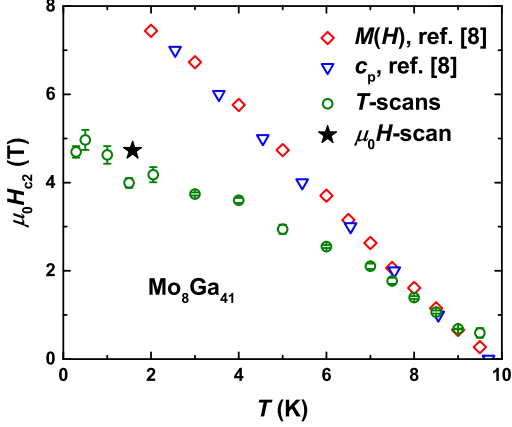


FIG. 6. Upper critical field $\mu_0 H_{c2}$ of $\text{Mo}_8\text{Ga}_{41}$ obtained from the T -scans and $\mu_0 H$ -scan. Values from the thermodynamic measurements⁸ are also shown.

in resolving the gap structure in $\text{Mo}_8\text{Ga}_{41}$ are highly desirable.

B. V for Mo substitution in $\text{Mo}_7\text{VGa}_{41}$

In our previous study⁸, $\text{Mo}_{8-x}\text{V}_x\text{Ga}_{41}$ was also found to be superconducting with the transition temperature T_c being just slightly lower than that for the parent compound. Zero-field and transverse-field μSR experiments were conducted therefore on $\text{Mo}_7\text{VGa}_{41}$ having $T_c \simeq 9.2$ K at zero magnetic field⁸. The analysis of the experimental data was performed similarly to that described previously for $\text{Mo}_8\text{Ga}_{41}$ sample.

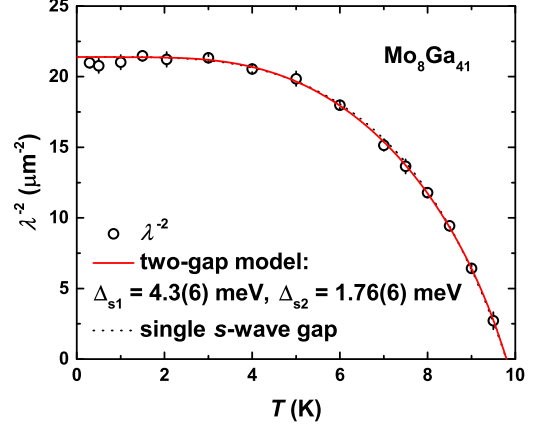


FIG. 7. Temperature-dependent magnetic penetration depth λ of $\text{Mo}_8\text{Ga}_{41}$ plotted as λ^{-2} vs. T . Solid line is a least-squares fit according to the two-gap model, the dashed line is a fit according to the single-gap BCS-type model.

Figure 8(a) shows a summary of the temperature-dependent upper critical field of $\text{Mo}_7\text{VGa}_{41}$. The $\mu_0 H_{c2}$ data from the magnetization and heat capacity experiments as well as that obtained in TF- μSR studies are presented. In contrast to the unsubstituted $\text{Mo}_8\text{Ga}_{41}$, the TF- μSR $\mu_0 H_{c2}$ values agree well with the data from thermodynamic measurements for $\text{Mo}_7\text{VGa}_{41}$. This implies that only one characteristic length scale is needed to describe the upper critical field. In accordance with this observation, the temperature dependence of the magnetic penetration depth of $\text{Mo}_7\text{VGa}_{41}$ presented as the $\lambda^{-2}(T)$ plot in Fig. 8(b) was satisfactorily fitted within the single-gap BCS-type model using Eq. (4). The fit

yields $\Delta(0) = 1.87(9)$ meV and $\lambda(0) = 292(4)$ nm with the value of $\Delta(0)/k_B T_c = 2.36$ exceeding the weak-coupling BCS limit of 1.76. Thus, from the TF- μ SR data we suggest a simple s -wave superconducting state in $\text{Mo}_7\text{VGa}_{41}$ accompanied by the strong electron-phonon coupling.

C. Comparison of $\text{Mo}_8\text{Ga}_{41}$ with its V-substituted analog $\text{Mo}_7\text{VGa}_{41}$

The experimental data presented above reveal that $\text{Mo}_8\text{Ga}_{41}$ and $\text{Mo}_7\text{VGa}_{41}$ are different in two important aspects. First of all, application of the equation of Brandt leads to different results. The Brandt equation (Eq. 3) is formulated for the case of single-gap s -wave superconductivity. By this reason, the values of $\mu_0 H_{c2}$ extracted for $\text{Mo}_7\text{VGa}_{41}$ using Eq. 3 are in good agreement with thermodynamic measurements, since $\text{Mo}_7\text{VGa}_{41}$ exhibits actually a single-gap s -wave superconductivity. The different situation is observed for $\text{Mo}_8\text{Ga}_{41}$. In this case, Eq. 3 yields the values of $\mu_0 H_{c2}$, which are significantly lower than those from thermodynamic measurements, indicating that $\text{Mo}_8\text{Ga}_{41}$ is not a single-gap superconductor. Fourier analysis of the asymmetry spectra reveals no signs of disorder of the vortex lattice that may cause the Brandt equation being not applicable. The $\lambda(\mu_0 H)$ dependence calculated using Eq. 3 also reveals the different behavior for $\text{Mo}_8\text{Ga}_{41}$ and $\text{Mo}_7\text{VGa}_{41}$ (Fig. 9). The field dependence of λ observed for $\text{Mo}_8\text{Ga}_{41}$ is reminiscent of that of NbSe_2 ¹⁷, which is also a two-gap superconductor¹⁸. At the same time, there is no field dependence in the case of $\text{Mo}_7\text{VGa}_{41}$ in compliance with its conventional behavior. The substitution of just one out of eight Mo atoms by one V atom leads to the *complete* suppression of one of the superconducting energy gaps.

The second aspect is that the V substitution is accompanied by more than a factor of 2 reduction of the superfluid density $\rho_s \propto \lambda^{-2}$. Indeed, from the fits of the experimental data we get $\lambda^{-2}(0) \simeq 21$ and $12 \mu\text{m}^{-2}$ for $\text{Mo}_8\text{Ga}_{41}$ and $\text{Mo}_7\text{VGa}_{41}$, respectively.

In order to explain such discrepancies, three different scenarios are going to be compared. According to the first one, the structural disorder caused by mixing Mo and V atoms in one crystallographic position may lead to the reduction in the superfluid density. From the single-crystal x-ray diffraction data⁸, it is known that the substitution occurs in two crystallographic positions, and the average V content is less than 15 at.%. Such small amount of disorder in the crystal structure should not cause a drastic change of ρ_s . Moreover, as in the case of the $\text{K}_{1-x}\text{Na}_x\text{Fe}_2\text{As}_2$ solid solution¹⁹, the reduction in ρ_s caused by structural disorder should be accompanied by the significant reduction in T_c , whereas the $\text{Mo}_{8-x}\text{V}_x\text{Ga}_{41}$ solid solution demonstrates no significant change of T_c . By substituting V for Mo, the transition temperature just slightly reduces from $T_c = 9.8$ K in $\text{Mo}_8\text{Ga}_{41}$ to 9.2 K in

$\text{Mo}_7\text{VGa}_{41}$ ⁸.

In contrast to $\text{K}_{1-x}\text{Na}_x\text{Fe}_2\text{As}_2$, the V for Mo substitution is not isovalent. Rather, the change in the electron count is observed, which enables us to formulate the second scenario, with the heterovalent substitution being responsible for the reduction in ρ_s . The effect of heterovalent substitution on the electronic structure of $\text{Mo}_{8-x}\text{V}_x\text{Ga}_{41}$ was analyzed in our previous study⁸. By using the rigid-band shift approximation, it was shown that no significant change in the density of states at the Fermi level occurs with increasing V content in the solid solution. Thus, the heterovalent nature of the substitution also does not explain the observed reduction in ρ_s .

Finally, the third scenario considers competing states that cause the reduction in the superfluid density ρ_s . The $\text{Ba}(\text{Fe}_{1-x}\text{Co}_x)_2\text{As}_2$ solid solution²⁰ is an example, in which the competition between superconductivity and magnetism is observed. On the phase diagram of $\text{Ba}(\text{Fe}_{1-x}\text{Co}_x)_2\text{As}_2$, the superconducting dome is intersected with the spin-density-wave field yielding the intermediate region of competing states. Measurements of the magnetic penetration depth λ clearly show that entering the intersected region results in the drastic increase in λ , which is equivalent to the reduction in ρ_s ²⁰.

At this point, we make an assumption that the emergence of some competing state in $\text{Mo}_7\text{VGa}_{41}$ may lead to the suppression of one of the superconducting gaps accompanied by the significant reduction in the superfluid density. The collected ZF- μ SR data show that both $\text{Mo}_8\text{Ga}_{41}$ and $\text{Mo}_7\text{VGa}_{41}$ ⁹ lack spontaneous coherent magnetic fields in the superconducting state, thus excluding magnetic order as a possible competing state from the consideration. To obtain further information, we analyze the low-temperature resistivity data⁸ for $\text{Mo}_8\text{Ga}_{41}$ and $\text{Mo}_7\text{VGa}_{41}$. The $\rho(T)$ data at low temperatures can be fitted using equation $\rho(T) = \rho_0 + AT^n$ (Figure 10). The fitting yields the exponents $n = 1.49(8)$ for $\text{Mo}_8\text{Ga}_{41}$ and $n = 1.21(3)$ for $\text{Mo}_7\text{VGa}_{41}$. This reduction in the exponent upon increasing V content may indicate the onset of an incipient charge-density-wave state in $\text{Mo}_7\text{VGa}_{41}$. A similar situation has been observed in $\text{Ta}_4\text{Pd}_3\text{Te}_{16}$ ²¹, where the suppression of n under pressure signifies enhancement of CDW fluctuations. The presence of CDW state in the V-substituted $\text{Mo}_8\text{Ga}_{41}$ would make one band unavailable for superconductivity and reduce the density of the supercarriers due to the opening of the energy gap associated with the CDW regime.

IV. CONCLUSIONS

A comprehensive study by means of muon spin rotation/relaxation technique was carried out on a strongly-coupled superconductor $\text{Mo}_8\text{Ga}_{41}$ and its V-substituted analog $\text{Mo}_7\text{VGa}_{41}$. ZF- μ SR experiments show that both compounds lack any spontaneous coherent magnetic fields in the superconducting state. TF- μ SR experiments elucidate microscopic properties of the superconducting

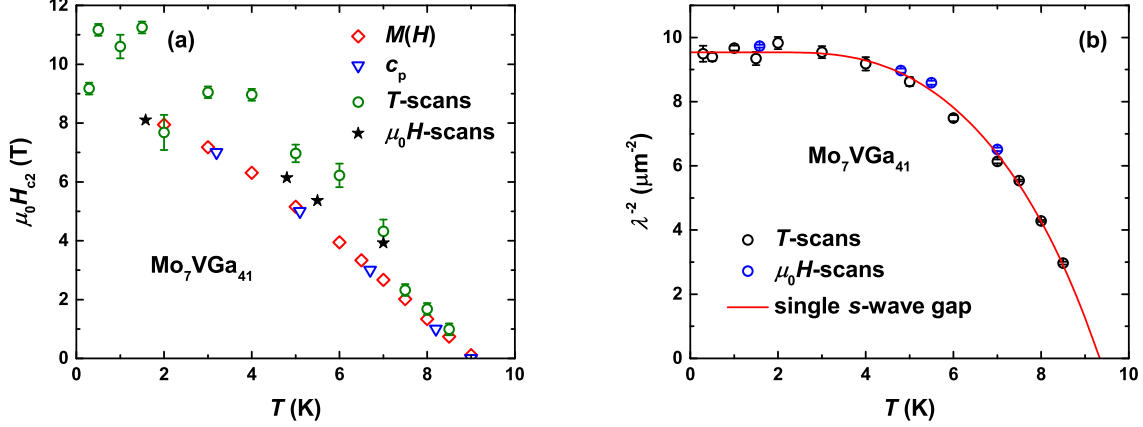


FIG. 8. (a) Upper critical field and (b) magnetic penetration depth of $\text{Mo}_7\text{VGa}_{41}$ plotted as λ^{-2} vs. T . Solid red line is a fit of the data according to the single-gap BCS-type model.

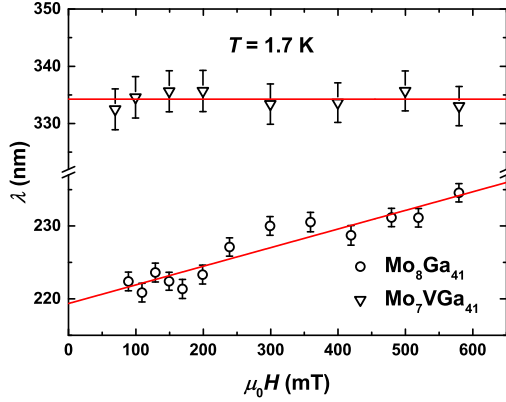


FIG. 9. Magnetic penetration depth λ as a function of magnetic field for $\text{Mo}_8\text{Ga}_{41}$ (open circles) and $\text{Mo}_7\text{VGa}_{41}$ (open triangles). The solid red lines are linear fits of the data.

state, which turns out to be substantially different in $\text{Mo}_8\text{Ga}_{41}$ and $\text{Mo}_7\text{VGa}_{41}$. The upper critical field of $\text{Mo}_8\text{Ga}_{41}$ extracted from the TF- μ SR data is lower than in thermodynamic measurements indicating the multigap superconductivity that leads to two or more independent length scales in the superconducting state. Accordingly, the temperature-dependent magnetic penetration depth was approximated by the model, in which two s -wave superconducting gaps with similar energies and almost equal contributions are assumed. The V for Mo substitution does not affect T_c significantly, but leads to the complete suppression of one superconducting gap. This follows from the substantial reduction in the superfluid density ρ_s and from the single-gap behavior of both the upper critical field and magnetic penetration depth of $\text{Mo}_7\text{VGa}_{41}$. We speculate that the emergence of a competing state in $\text{Mo}_7\text{VGa}_{41}$ is responsible for the closure

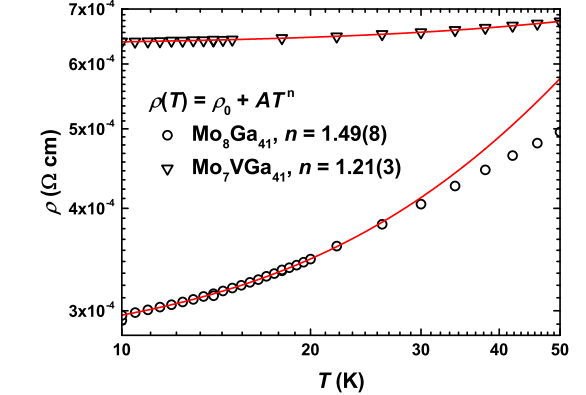


FIG. 10. Resistivity of $\text{Mo}_8\text{Ga}_{41}$ (open circles) and $\text{Mo}_7\text{VGa}_{41}$ (open triangles) at low temperatures. The data are taken from ref. [8]. Solid red lines are the results of fitting (see in the text).

of one of the superconducting gaps.

ACKNOWLEDGMENTS

This work was performed at the Swiss Muon Source, Paul Scherrer Institute, Villigen, Switzerland. Part of the experimental work was done by Gustavo Prack, Judith Suter and Clemens Spinnler (Swiss Nanoscience Institute, University of Basel, Basel, Switzerland) within their lab course at PSI. R.K. acknowledges Stefan Holenstein and Jean-Christophe Orain for their help during the μ SR experiments. The work has been supported by the Russian Science Foundation, grant #17-13-01033. V.Yu.V. appreciates the support from the European Regional Development Fund, project TK134. A.A.T. is grateful for

the financial support by the Federal Ministry for Educa-

tion and Research under the Sofja Kovalevskaya Award of the Alexander von Humboldt Foundation.

-
- * verchenko@inorg.chem.msu.ru
 † rustem.khasanov@psi.ch
- ¹ W. Xie, H. Luo, B. F. Phelan, T. Klimczuk, F. A. Cevallos, and R. J. Cava, *PNAS* **112**, 7048 (2015).
 - ² A. Bezinge, K. Yvon, M. Decroux, and J. Muller, *J. Less-Common Met.* **99**, L27 (1984).
 - ³ C. P. Poole, *Handbook of superconductivity* (Academic Press, London, 2000).
 - ⁴ T. Shibayama, M. Nohara, H. A. Katori, Y. Okamoto, Z. Hiroi, and H. Takagi, *J. Phys. Soc. Jpn.* **76**, 073708 (2007).
 - ⁵ K. Girgis, W. Petter, and G. Pupp, *Acta Cryst. B* **31**, 113 (1975).
 - ⁶ Y. Grin, K. Peters, and H. G. von Schnering, *Z. Crystallogr.* **212**, 6 (1997).
 - ⁷ K. Yvon, *Acta Cryst.* **B31**, 117 (1975).
 - ⁸ V. Y. Verchenko, A. A. Tsirlin, A. O. Zubtsovskiy, and A. V. Shevelkov, *Phys. Rev. B* **93**, 064501 (2016).
 - ⁹ Specimen characterization, ZF- μ SR, and TF- μ SR data on the Mo₇VGa₄₁ sample are presented as Supplemental materials.
 - ¹⁰ R. Kubo, *Hyperfine interact.* **8**, 731 (1981).
 - ¹¹ D. A. Cardwell and D. S. Ginley, *Handbook of superconducting materials* (CRC Press, London, 2002).
 - ¹² E. H. Brandt, *Phys. Rev. B* **68**, 054506 (2003).
 - ¹³ S. Lee, R. Cywinski, and S. Kilcoyne, *Muon Science: Muons in Physics, Chemistry and Materials* (CRC Press, London, 1999).
 - ¹⁴ M. Tinkham, *Introduction to Superconductivity: Second Edition* (Dover Publications, Mineola, 2004).
 - ¹⁵ H. Padamsee, J. E. Neighbor, and C. A. Shiffman, *J. Low Temp. Phys.* **12**, 387 (1973).
 - ¹⁶ R. Khasanov, A. Amato, P. K. Biswas, H. Luetkens, N. D. Zhigadlo, and B. Batlogg, *Phys. Rev. B* **90**, 140507(R) (2014).
 - ¹⁷ J. E. Sonier, R. F. Kiefl, J. H. Brewer, J. Chakhalian, S. R. Dunsiger, W. A. MacFarlane, R. I. Miller, A. Wong, G. M. Luke, and J. W. Brill, *Phys. Rev. Lett.* **79**, 1742 (1997).
 - ¹⁸ C. L. Huang, J.-Y. Lin, Y. T. Chang, C. P. Sun, H. Y. Shen, C. C. Chou, H. Berger, T. K. Lee, and H. D. Yang, *Phys. Rev. B* **76**, 212504 (2007).
 - ¹⁹ H. Kim, M. A. Tanatar, Y. Liu, Z. C. Sims, C. Zhang, P. Dai, T. A. Lograsso, and R. Prozorov, *Phys. Rev. B* **89**, 174519 (2014).
 - ²⁰ R. T. Gordon, H. Kim, N. Salovich, R. W. Giannetta, R. M. Fernandes, V. G. Kogan, T. Prozorov, S. L. Bud'ko, P. C. Canfield, M. A. Tanatar, and R. Prozorov, *Phys. Rev. B* **82**, 054507 (2010).
 - ²¹ J. Pan, W. H. Jiao, X. C. Hong, Z. Zhang, L. P. He, P. L. Cai, J. Zhang, G. H. Cao, and S. Y. Li, *Phys. Rev. B* **92**, 180505(R) (2015).